Electronic Supplementary Information

Sulfur-bridge ligands altering the microenvironment of single-atom CoN_3S sites to boost oxygen reduction reaction

Feng Liu,[a] Yingchun Guo,*[b] Yan Zhong,[a] Jingsha Li,[a] Heng Zhang,[a] Lei Shi,[c] Xuanni Lin,[d] Fenghui Ye,[d] Kai Ge,[e] Shuai Yuan,[f] Chuangang Hu*[d] and Chunxian Guo*[a]

[a] Institute of Materials Science and Devices, School of Materials Science and Engineering, Suzhou University of Science and Technology, Suzhou 215009, China.

[b] Department of Materials Engineering, Huzhou University, Huzhou 313000, China.

[c] CAS Key Laboratory of Nanosystem and Hierarchical Fabrication, CAS Center for Excellence in Nanoscience, National Center for Nanoscience and Technology, Beijing 100190, China.

[d] State Key Laboratory of Organic-Inorganic Composites, College of Chemical Engineering, Beijing University of Chemical Technology, Beijing 100029, China.

[e] Institute of Polymer Science and Engineering, Hebei Key Laboratory of Functional Polymers, Hebei University of Technology, Tianjin 300130, China.

[f] School of Software and Microelectronics, Peking University, Beijing 102600, China.

*Corresponding authors

E-mail: cxguo@usts.edu.cn (C. Guo)

ycguo@zjhu.edu.cn (Y. Guo)

chuangang.hu@mail.buct.edu.cn (C. Hu)

Experimental Section

Preparation of Co-ZIF-8. 2.232 g (7.503 mmol) zinc nitrate and 0.117 g (0.402 mmol) cobalt nitrate were dissolved in 50 mL methanol as solution A; 4.885 g (0.0595 mol) 2-methimidazole were dissolved in 50 mL methanol, named solution B, solution A was poured into solution B, adjusting the reaction speed to 800 rpm for 24 h. The resulting solution was centrifuged at 12,000 rpm for 2 min, washed twice with methanol, and finally dried in vacuum at 60 °C. The obtained product was denoted as Co-ZIF-8.

Preparation of MS@Co-ZIF-8. Thiourea (4 mg) and 4 μL thiophene was dissolved in 10 ml of ethanol and quickly poured into the Co-ZIF-8 ethanol dispersion (200 mg/20 ml) with vigorous magnetic stirring for 5 h. The resultant solution was centrifuged at 12,000 rpm for 2 min, rinsed with ethanol, and then vacuum-dried at 60 °C, obtaining MS@Co-ZIF-8.

Preparation of Co-N/S-C and C-N/C. The precursor MS@Co-ZIF-8 and Co-ZIF-8 were heat-treated at 950 °C in Ar atmosphere for 2 hours with a heating rate of 5 °C min^{-1} and then naturally cooled to room temperature, respectively. The resulted product were denoted as Co-N/S-C and Co-N/C, respectively.

Materials Characterization. Scanning electron microscopy (SEM) images were obtained from Zeiss Gemini 300 scanning electron microscope. Transmission electron microscopy (TEM), high resolution transmission electron microscopy (HRTEM), selected area electron diffraction (SEAD), high-annular dark-field scanning TEM (HAADF-STEM), and EDS were conducted on a JEOL JEM-2200FS transmission electron microscope. Aberration-corrected High-angle annular dark-field scanning transmission electron microscopy (HAADF-STEM) images were performed with a JEOL JEM-ARM 200F transmission electron microscope with a probe corrector operated at 200 kV. The X-ray absorption fine structure spectra (XAFS) spectra at the Fe K-edge were measured at 1W1B station in Beijing Synchrotron Radiation Facility (BSRF, operated at 2.5 GeV with a maximum current of 250 mA). The spectra of

samples were recorded in fluorescence excitation mode using a Lytle detector. The spectra of Co foil and Co_3O_4 were used as references, and recorded in a transmission mode using ionization chamber. The crystal phases of the samples were characterized by a Bruker D2 Phaser X-ray diffractometer with a Cu Kα radiation source (30 kV, 10 mA). Raman spectra were recorded using a Horibal LabRAM HR Evolution Raman spectrometer operating with a laser wavelength of 532 nm. The nitrogen adsorption and desorption isotherms were studied by using a Micrometrics ASAP 2460 Specific surface and porosity analyzer. The specific surface area and pore size distribution were calculated from the nitrogen adsorption-desorption isotherms. X-ray photoelectron spectroscopy (XPS) measurements were carried out on a Kratos AXIS SUPRA X-ray photoelectron spectrometer with an Al Kα radiation (15 kV, 10 mA).

Electrochemical Measurements. The oxygen reduction reaction (ORR) activities of catalysts were measured by a CHI Electrochemical workstation (model 760c) with a standard three-electrode system at room temperature. The catalyst-coated glassy carbon rotating disk electrode (RDE, 5 mm in diameter) or rotating ring-disk electrode (RRDE, disk outer diameter, ring inner diameter and ring outer diameter are 5.61 mm, 6.25 mm, and 7.92 mm, respectively) was used as the working electrode, an Ag/AgCl electrode in saturated KCl solution was used as the reference electrode, and graphite rod was used as counter electrode. All of the potentials reported in this paper were calibrated to the reversible hydrogen electrode. To prepare a homogeneous catalyst ink, 3 mg of catalyst was dispersed in a solution of 147 μL of deionized water, 147 μL of isopropanol and 6 μL of a Nafion solution (5 wt%, Alfa Aesar D521) under sonication for 2 h. Then 7.5 μL of catalyst ink were loaded onto the glassy carbon and dried in air. A Pt/C (20 wt% of Pt, Johnson Mattery HiSPEC) catalyst with a loading of 40 μg_{Pt} cm^{-2} was used as a reference. Linear scan voltammetry (LSV) tests were carried out in O_2-saturated 0.1 M KOH solution with a scan rate of 5 mV s^{-1}. The LSV curves of all catalysts were subtracted the background current measured under nitrogen atmosphere. In the accelerated stability test (ADT), cyclic voltammetry (CV) measurements were performed in O_2-saturated 0.1 M KOH solution with a sweep rate

of 50 mV s^{-1}. Four-electron selectivity during the ORR was determined by measuring LSV curves on RDE at various rotating speeds (625, 900, 1225, 1600, and 2025 rpm). The corresponding electron transfer number was determined from the slope of the linear line according to the following Koutechy-Levich (K-L) equation:

$$\frac{1}{J} = \frac{1}{J_L} + \frac{1}{J_K} = \frac{1}{B\omega^{1/2}} + \frac{1}{J_K}$$

$$B = 0.62nF(D_0)^{2/3}(\nu)^{-1/6}C_0 \quad (1)$$

where J, J_L, J_K are the measured current density, diffusion-limiting current density, and kinetic current density, respectively. ω is the angular velocity of the disk ($\omega = 2\pi N$, N is the rotation speed), n is the electron transfer number, F is the Faraday constant (F = 96,485 C mol^{-1}), D_0 is the diffusion coefficient of oxygen ($D_0 = 1.9 \times 10^{-5}$ cm^2 s^{-1}, 0.1 M KOH), C_0 is the bulk concentration of oxygen ($C_0 = 1.2 \times 10^{-6}$ mol cm^{-3}, 0.1 M KOH), ν is the kinetic viscosity of the electrolyte (ν = 0.01 cm^2 s^{-1}). The electron transfer number (n) and the yield of H_2O_2 were calculated from the RRDE measurement based on the disk current (I_d) and ring current (I_r) via the following equations:

$$n = 4 \times \frac{I_d}{I_d + I_r / N} \quad (2)$$

$$H_2O_2\% = 200 \times \frac{I_r}{(I_r + NI_d)} \quad (3)$$

Where N = 0.37 is the current collection efficiency of Pt ring.

TOF calculation. The turnover frequency (TOF) of the catalysts were calculated from the following equation:

$$TOF = \frac{J_k \times N_e}{\omega_{Co} \times C_{cat} \times N_A / M_{Co}} \quad (4)$$

Where J_k is the kinetic current density (A cm^{-2}), N_e is electron number per Coulomb 6.24×10^{18}, ω_{Co} is the metal content in the catalyst, C_{cat} is the catalyst loading on the electrode, N_A is Avogadro constant 6.022×10^{23}, M_{Co} is molar mass of Co 58.93 g

mol^{-1}.

Zn-air battery test. The home-made zinc-air battery device has been employed for the battery performance measurements. The electrolyte used for the electrochemical liquid zinc-air battery was 6 M KOH and 0.2 M $Zn(Ac)_2$ aqueous solution. Typically, 5 mg catalysts mixed with 20 μL Nafion solution (5 wt%, Alfa Aesar D521) were dispersed in 490 μL of deionized water and 490 μL of isopropanol solution by sonicating for 2 h to form a homogeneous ink. The obtained catalyst ink was then brushed onto a piece of carbon paper with an effective area of 1 cm^2 until the loading amount reaching 1 mg cm^{-2}, which was serving as the cathode for Zn-air battery. A polished zinc plate (0.1 mm thickness) was used as the anode. As a reference material, 20 wt% Pt/C catalysts were prepared as the same procedure and the Pt/C loading on the carbon was 1.0 mg cm^{-2}. All the Zn-air batteries were tested under ambient atmosphere. Discharge polarization and power density curves were measured on CHI 760E electrochemical workstation (CHI Instruments, Inc., Shanghai). The glavanostatic discharge test were performed on a LAND CT2001A testing system.

Computational details. The density functional theory (DFT) calculations were carried out using the DMol3[1] module implemented in Material Studio. The GGA method as implemented with Perdew, Burke, and Ernzerhof (PBE-GGA)[2, 3] was used to describe the exchange-correlation functional component of the Hamiltonian. The k point grids were set as 2 × 2 × 1 for the Brillouin zone and a large vacuum slab of 15 Å is inserted in z direction for surface isolation to prevent interaction between two neighboring surfaces. The convergence threshold for the iteration in self-consistent-field (SCF) is set to be 10^{-5} eV. A smearing of 0.005 Ha (1 Ha = 27.21 eV) to the orbital occupation was applied. The geometry convergence tolerance for energy change, max force and max displacement were 1×10^{-5} Ha, 0.002 Ha/Å, 0.005 Å, respectively.

The ORR proceeds for four-electron pathway in alkaline electrolyte are shown as follows:[4]

$$* + O_2 + H_2O + e^- \rightarrow OOH* + OH^- \quad (5)$$

$$OOH^* + e^- \rightarrow O^* + OH^- \quad (6)$$

$$O^* + H_2O + e^- \rightarrow OH^* + OH^- \quad (7)$$

$$OH^* + e^- \rightarrow * + OH^- \quad (8)$$

Where * refers to an active site on the catalysts surface.

The reaction Gibbs free energy changes (ΔG) were calculated by the following equation:

$$\Delta G = \Delta E + \Delta ZPE - T\Delta S + \Delta G_{pH} + \Delta G_U \quad (9)$$

Where ΔE is obtained directly from DFT calculation results, ΔZPE is the correction of zero point vibration energy (ZPE), T is the room temperature of 298.15K, and ΔS is the correction for entropy. $\Delta G_{pH} = -K_B T \ln[H^+] = pH \times K_B T \ln 10$,[5] is the change of free energy owing to the effect of pH value of the electrolyte. $\Delta G_U = -neU$, is the effect of the electrons transfer in the electrode and the electrode potential contribution to ΔG.

Supplementary Figures

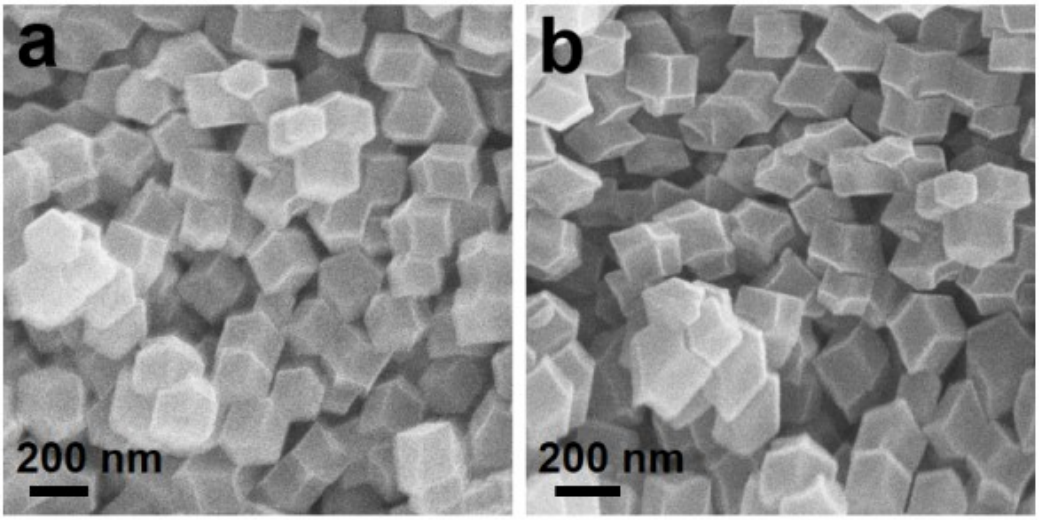

Fig. S1. (a, b) SEM images of Co-ZIF-8 and MS@Co-ZIF-8.

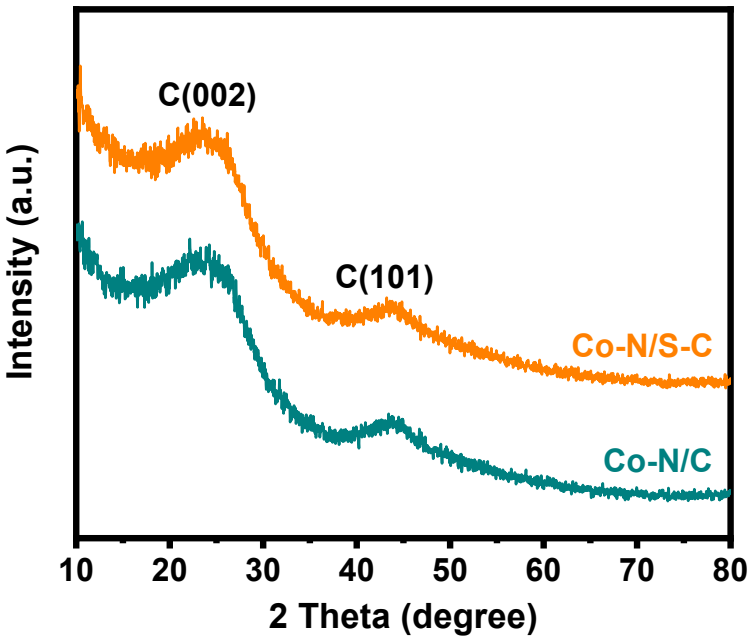

Fig. S2. XRD patterns of Co-N/S-C and Co-N/C.

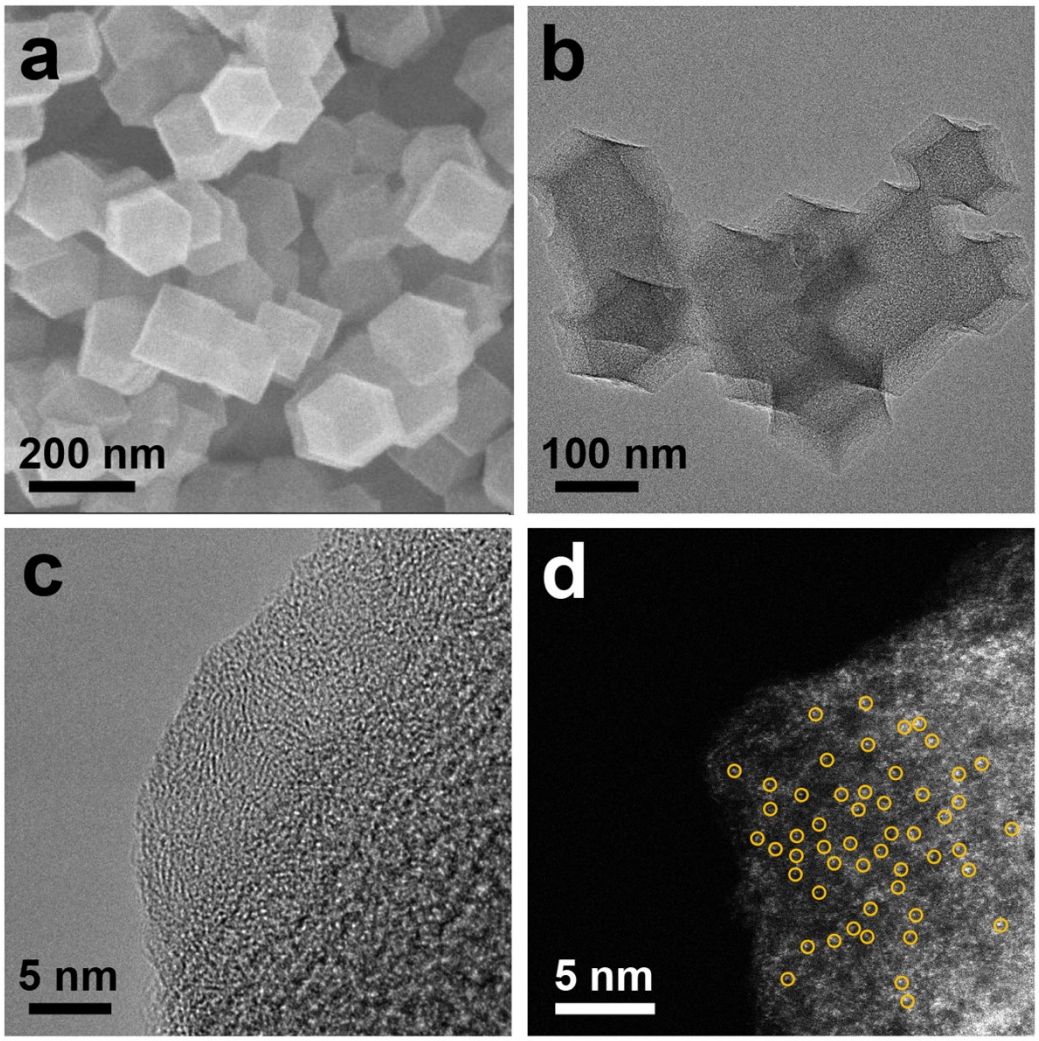

Fig. S3 (a) SEM and (b) TEM images of Co-N/C. (c) HRTEM and (d) AC HAADF-STEM images of Co-N/C.

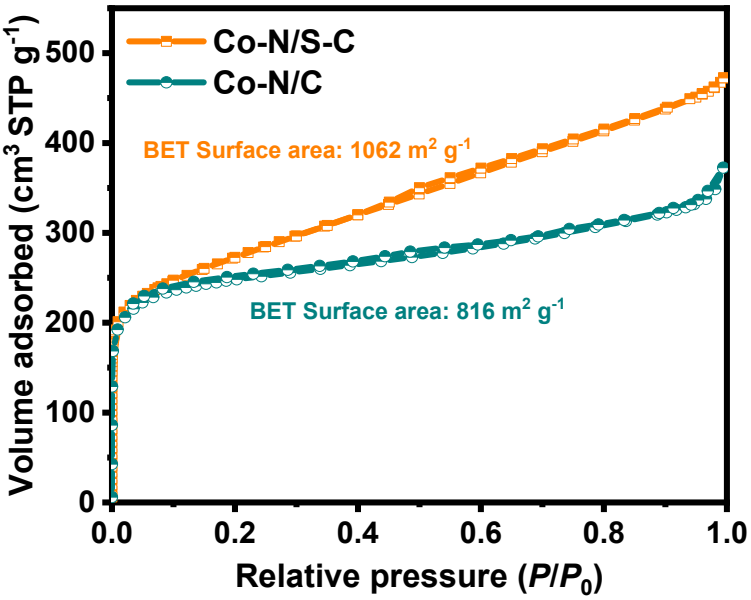

Fig. S4. N_2 adsorption-desorption isotherms of Co-N/S-C and Co-N/C.

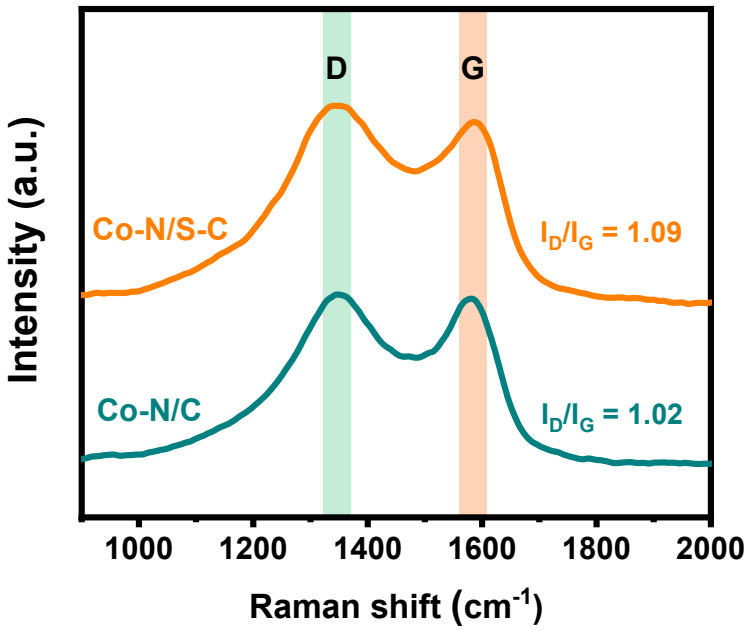

Fig. S5. Raman spectra of Co-N/S-C and Co-N/C.

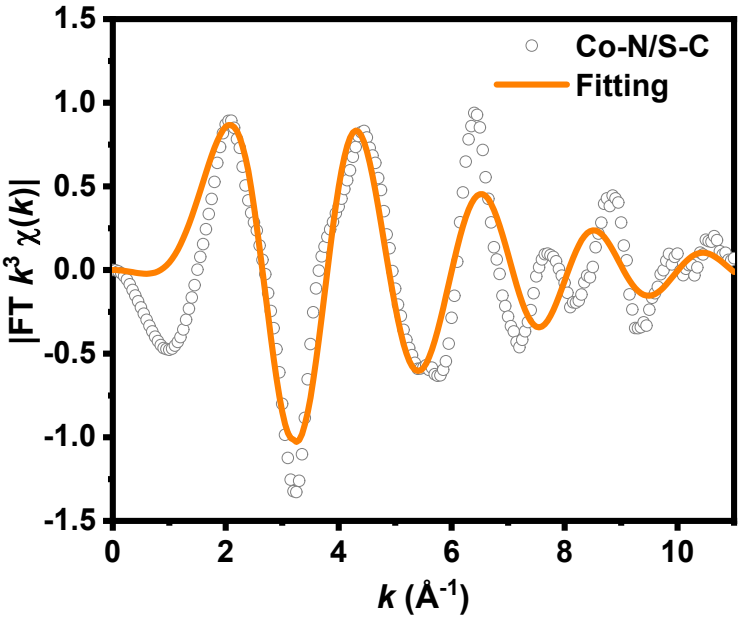

Fig. S6. The corresponding FT-EXAFS k-space fitting curve of Co-N/S-C.

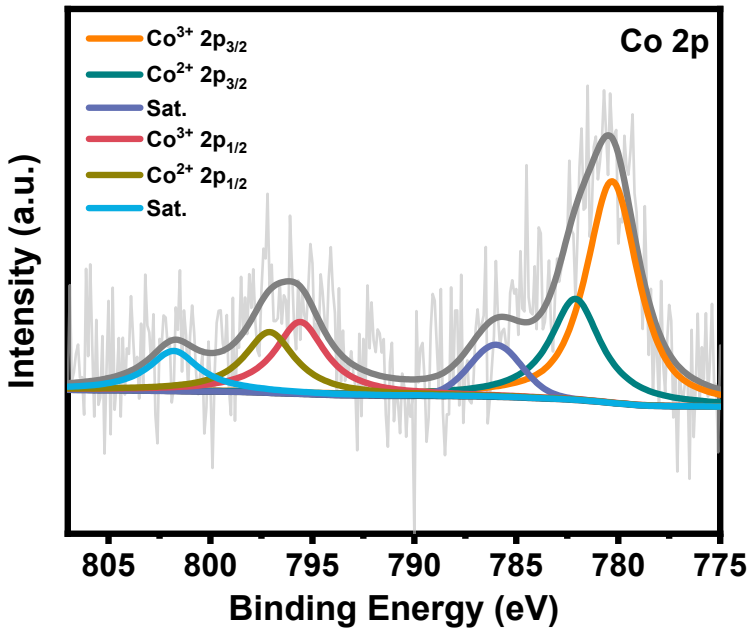

Fig. S7. High-resolution Co 2p XPS spectrum of Co-N/C.

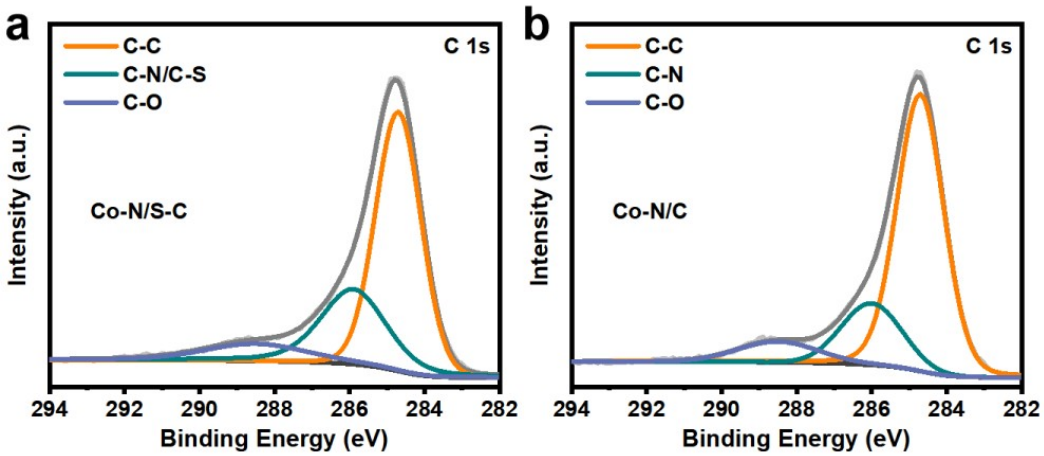

Fig. S8. High-resolution C 1s XPS spectra of (a) Co-N/S-C and (b) Co-N/C.

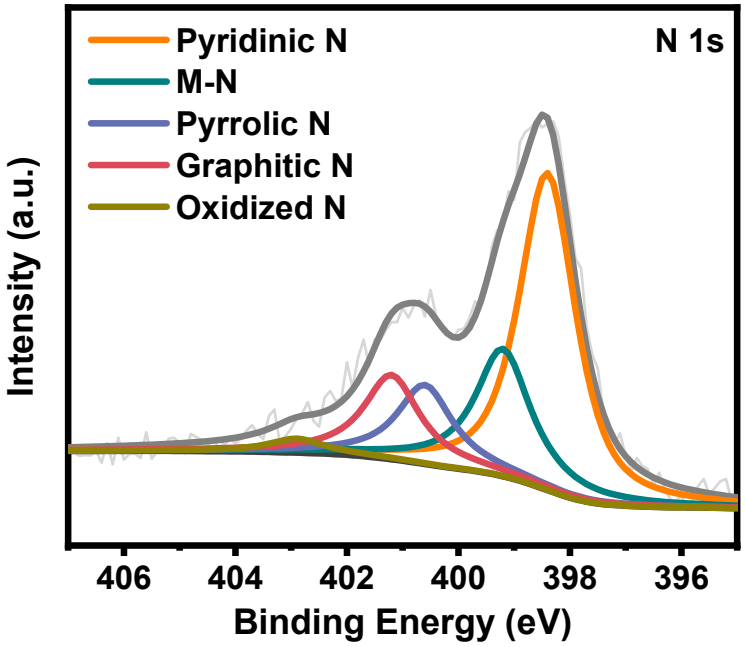

Fig. S9. High-resolution N 1s XPS spectrum of Co-N/C.

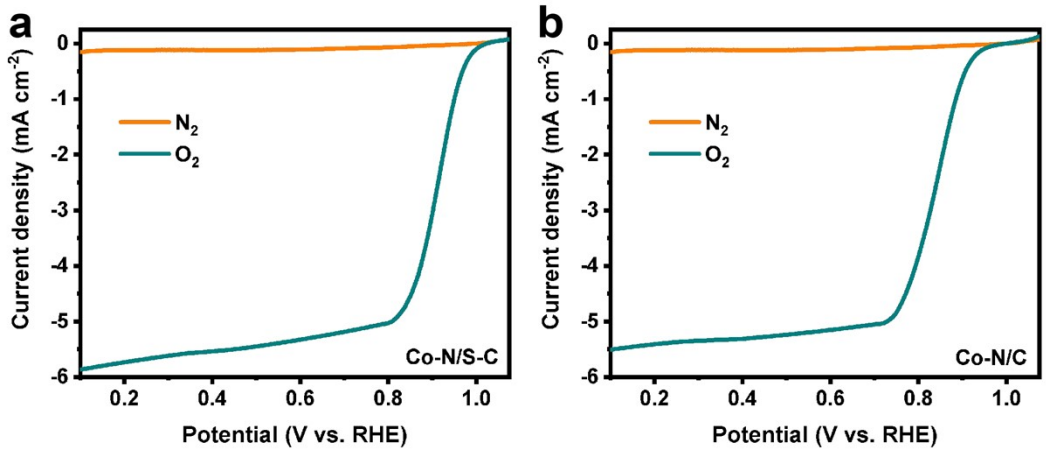

Fig. S10. ORR polarization curves of (a) Co-N/S-C and (b) Co-N/C in N_2 and O_2-saturated 0.1 M KOH solution with a scan rate of 5 mV S^{-1} and a rotation rate of 1600 rpm.

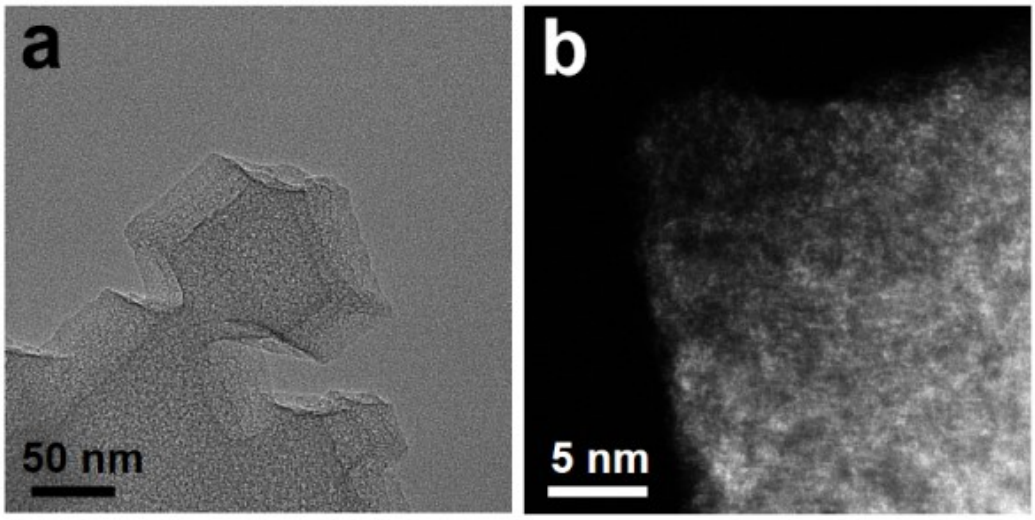

Fig. S11. (a) TEM and (b) AC HAADF-STEM images of the used Co-N/S-C after durability test.

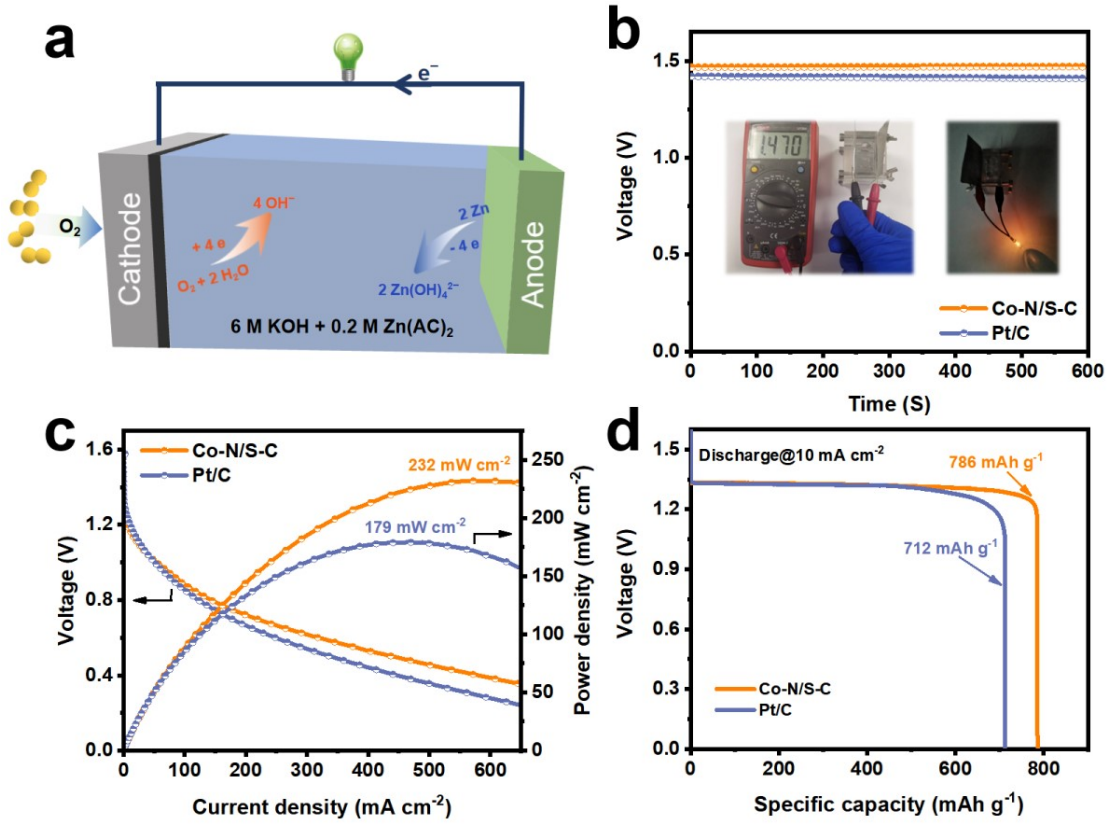

Fig. S12. (a) Schematic diagram of Zn-air battery. (b) Open-circuit potentials (OCV) of Zn-air batteries with Co-N/S-C and Pt/C as the air cathode catalysts, respectively. Inset: the photograph of Zn-air battery with Co-N/S-C showing the OCV of 1.47 V and a photograph of a yellow LED powered by a home-made Zn-air battery utilizing Co-N/S-C catalyst. (c) Polarization and power density curves of Co-N/S-C and Pt/C-based Zn-air batteries. (d) Galvanostatic discharge curves of the Zn-air batteries at 10 mA cm^{-2}.

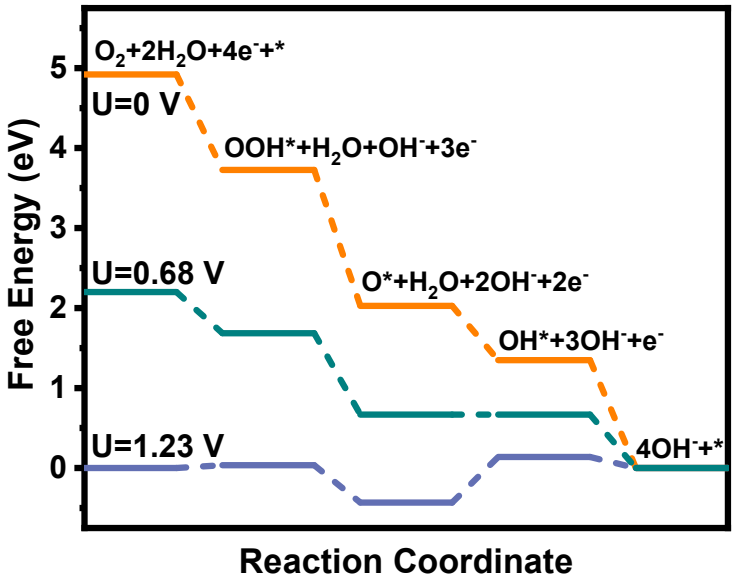

Fig. S13. ORR free-energy diagrams of CoN_4C_{10} model.

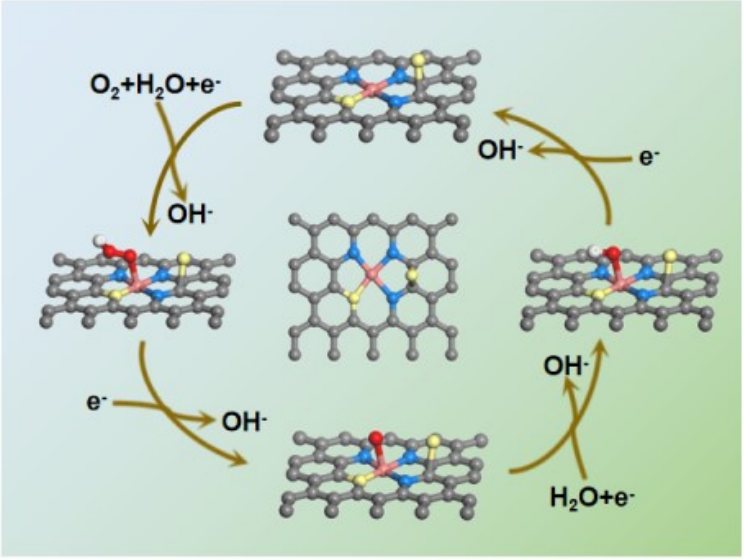

Fig. S14. Proposed ORR mechanism on the CoN_3SC_{10}-S site.

Supplementary Tables

Table S1. The values of specific surface area, total pore volume and micropore volume of Co-N/S-C and Co-N/C catalysts.

Sample	S_{BET} (m^2 g^{-1})	Total pore volume (cm^3 g^{-1})	Micropore volume (cm^3 g^{-1})
Co-N/S-C	1062	0.59	0.41
Co-N/C	816	0.50	0.35

Table S2. EXAFS fitting parameters at the Co K-edge for Co-N/S-C (S_0^2 = 0.82).

Sample	Scattering pair	CN	R(Å)	$\sigma^2(10^{-3}Å^2)$	ΔE_0(eV)	R factor
Co-N/S-C	Co-N	3.1	1.98	4.9	1.3	0.011
	Co-S	1.1	2.31	5.2		

N, coordination number; R, bonding distance; σ^2, Debye-Waller factor; ΔE_0, edge-energy shift; R factor is used to value the goodness of the fitting. Error bars that characterize the structural parameters obtained by EXAFS spectroscopy were estimated as CN ± 20%; R ± 1%; σ^2 ± 20%; ΔE_0 ± 20%.

Table S3. XPS elemental quantification of Co-N/S-C and Co-N/C catalysts.

Sample	C (at%)	N (at%)	O (at%)	Co (at%)	S (at%)
Co-N/S-C	81.55	8.85	8.72	0.67	0.21
Co-N/C	81.31	8.69	9.27	0.73	/

Table S4. ORR activity comparison of Co-N/S-C with previously reported highly active non-precious metal catalysts.

Catalyst	Loading (mg cm^{-2})	Electrolyte	$E_{1/2}$ (V vs. RHE)	Reference
Co-N/S-C	**0.38**	**0.1 M KOH**	**0.908**	**This work**
HCNT@Co-NC	0.4	0.1 M KOH	0.85	*Chem. Commun.* **2024**, 60, 1476-1479.
FeNC-VN	0.3	0.1 M KOH	0.902	*J. Am. Chem. Soc.* **2024**, 146, 4803-4813.
FeN_4-Fe_{NCP}@MCF	0.3	0.1 M KOH	0.894	*Adv. Funct. Mater.* **2024**, 2315150.
T-Fe SAC	0.2	0.1 M KOH	0.91	*Angew. Chem. Int. Ed.* **2024**, 63, e202319370.
H-3DOM-Co/ONC	0.2	0.1 M KOH	0.84	*Adv. Mater.* **2023**, 35, 2301894.
P-O/FeNC-SAC	0.27	0.1 M KOH	0.912	*ACS Energy Lett.* **2023**, 8, 4531-4539.
MnSA/MnAC-SSCNR	-	0.1 M KOH	0.90	*Small* **2023**, 2309727.
FeN_4Cl-SAzyme	-	0.1 M KOH	0.885	*Chem. Commun.* **2023**,59, 3550-3553.
Sb_1/NG(O)	0.255	0.1 M KOH	0.86	*Angew. Chem. Int. Ed.* **2022**, 61, e202202200.
Mn SAs/Fe_3C NPs@NPC	0.5	0.1 M KOH	0.88	*Nano Res.* **2022**, 15, 7976-7985.
Mn-SA@CNSs	0.255	0.1 M KOH	0.88	*Energy Storage Mater.* **2022**, 49, 209-218.
Ru-SAS/SNC	0.4	0.1 M KOH	0.861	*J. Am. Chem. Soc.* **2022**, 144, 2197-2207.
Co-CMS	0.2	0.1 M KOH	0.83	*Adv. Energy Mater.* **2022**, 12, 2103097.
V-N-C SAC	0.4	0.1 M KOH	0.858	*Chem. Eng. J.* **2022**, 444, 136363.
r-Fe-NC	0.6	0.1 M KOH	0.90	*Sci. Bull.* **2022**, 67, 1264-1273.
FeCo-N-HCN	0.102	0.1 M KOH	0.86	*Adv. Funct. Mater.* **2021**, 2011289.
Fe SA-NSC-900	0.1	0.1 M KOH	0.86	*ACS Energy Lett.* **2021**, 6, 379-386.
meso-Fe-N-C	0.4	0.1 M KOH	0.846	*ACS Catal.* **2021**, 11, 74-81.
Co_1-N_3PS/HC	0.51	0.1 M KOH	0.92	*Angew. Chem. Int. Ed.*

				2021, 60, 3212-3221.
CoNC@LDH	0.25	0.1 M KOH	0.84	*Adv. Mater.* **2021**, 2008606.
Fe/OES	0.4	0.1 M KOH	0.85	*Angew. Chem. Int. Ed.* **2020**, 132, 7454-7459.
Fe-N/P-C-700	0.6	0.1 M KOH	0.867	*J. Am. Chem. Soc.* **2020**,142, 2404-2412.
Fe/OES	0.4	0.1 M KOH	0.85	*Angew. Chem. Int. Ed.* **2020**, 132, 7454-7459.

References

[1] B. Delley, *J. Chem. Phys.* **2000**, *113*, 7756.

[2] J. P. Perdew, K. Burke and M. Ernzerhof, *Phys. Rev. Lett.* **1996**, *77*, 3865.

[3] J. P. Perdew, K. Burke and M. Ernzerhof, *Phys. Rev. Lett*. **1997**, *78*, 1396.

[4] Z. Yang, Y. Wang, M. Zhu, Z. Li, W. Chen, W. Wei, T. Yuan, Y. Qu, Q. Xu, C. Zhao, X. Wang, P. Li, Y. Li, Y. Wu, Y. Li, *ACS Catal.* **2019**, *9*, 2158.

[5] J. K. Norskov, J. Rossmeisl, A. Logadottir, L. Lindqvist, J. R. Kitchin, T. Bligaard, H. Jonsson, *J. Phys. Chem. B* **2004**, *108*, 17886.